The Journal of Adhesion, 83:679–704, 2007

ISSN: 0021-8464 print/1545-5823 online
DOI: 10.1080/00218460701490348

Taylor & Francis
Taylor & Francis Group

Critical Confinement and Elastic Instability in Thin Solid Films

Animangsu Ghatak
Department of Chemical Engineering, Indian Institute of Technology, Kanpur, India

Manoj K. Chaudhury
Department of Chemical Engineering, Lehigh University, Bethlehem, Pennsylvania, USA

When a flexible plate is peeled off a thin and soft elastic film bonded to a rigid support, uniformly spaced fingering patterns develop along their line of contact. Although the wavelength of these patterns depends only on the thickness of the film, their amplitude varies with all material and geometric properties of the film and that of the adhering plate. Here we have analyzed this instability by the regular perturbation technique to obtain the excess deformations of the film over and above the base quantities. Furthermore, by calculating the excess energy of the system, we have shown that these excess deformations, associated with the instability, occur for films that are critically confined. We have presented two different experiments for controlling the degree of confinement: by prestretching the film and by adjusting the contact width between the film and the plate.

Keywords: Adhesion; Bifurcation; Confinement; Elastic instability; Pattern formation; Thin soft films

INTRODUCTION

Pattern formation by self-organization is a subject of much interest because of its immense scientific and technological importance. Although examples of instability-driven evolution of such patterns abound in dynamic systems involving viscous and viscoelastic

Received 20 March 2007; in final form 14 May 2007.
One of a Collection of papers honoring Liliane Léger, the recipient in February 2007 of *The Adhesion Society Award for Excellence in Adhesion Science, Sponsored by 3M*.
Address correspondence to Animangsu Ghatak, Department of Chemical Engineering, Indian Institute of Technology, Kanpur 208016, India. E-mail: aghatak@iitk.ac.in

materials [1–10], such instances reported for purely elastic solids are rather scanty. Recently, such a pattern-forming system has been identified [11–13] with thin, soft elastic films confined between rigid or flexible substrates. Here the patterns of instability appear when a flexible plate is peeled off a layer of elastic adhesive bonded to a rigid substrate, resulting in undulations along their line of contact. Neither the appearance of these patterns nor their wavelength depend on the rate of peeling, thus remaining independent of the dynamics of the system. Indeed, the morphology does not exhibit any temporal evolution even when the contact line comes to a complete rest. The elastic nature of the film allows us to form the patterns repeatedly on the same film, so that similar patterns can be replicated many times. Looking at the prospect of this instability being used as a powerful pattern-forming tool, we have studied it extensively [14] in a variety of experimental geometries as well as with adhesives and adherents with varying material and physical properties. We have also developed methods to fix permanently these patterns [15].

In these experiments, a layer of elastic film of thickness, h, and shear modulus, μ, remains strongly bonded to a rigid substrate, and a microscope cover slip of flexural rigidity, D, is peeled off it by inserting a spacer at the opening of the crack. The patterns appear in the form of well-defined undulations at the contact line. Although the wavelength, λ, of these waves increases linearly with the thickness, h, of the film, remaining independent of its shear modulus, μ, and the flexural rigidity, D, of the plate, the amplitude, A, varies rather nonlinearly with these parameters. For the sake of systematic presentation of these results, we have introduced a confinement parameter $\varepsilon = hq$ [16] defined as the ratio of two different length scales: thickness h and $q^{-1} = (Dh^3/3\mu)^{1/6}$ [17,18], the latter being the stress decay length along the film/plate interface from the contact line (along the negative x direction in Fig. 1a). These definitions imply that the lower the value of ε, the longer the stress decay length for a film of a given thickness; hence, more confined is the film. For large values of ε, *i.e.*, low levels of confinement, the film can compensate its stretching perpendicular to the interface *via* lateral Poisson contraction. However, when ε decreases to less than a critical value ($\varepsilon < 0.35$), the films cannot afford a large-scale Poisson contraction. Then, to accommodate lateral contraction at a local level, the contact line turns undulatory to engender uniformly spaced fingers and cavities. In this report, we present two different experimental schemes to demonstrate how the confinement can be controlled in a systematic way. In one experiment, a flexible plate is lifted off a thin elastic film from both of its ends, thus effecting an adjustable contact width between the two, whereas in the

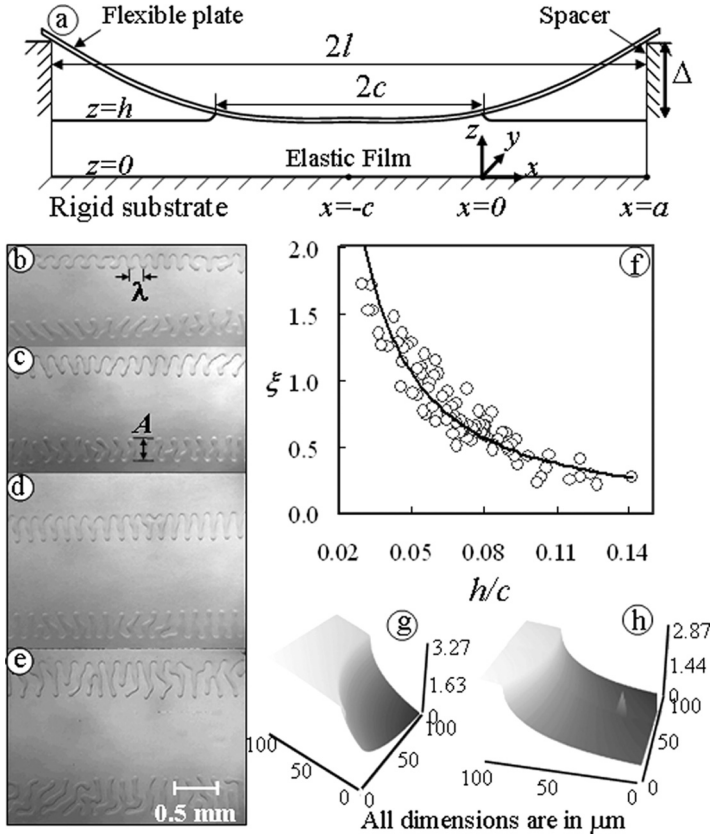

FIGURE 1 (a) Two-dimensional sketch (figure not drawn according to scale) of the experiment in which a flexible glass plate (silanized with self-assembled monolayers of hexadecyltrichlorosilane) is peeled off an elastic film of cross-linked poly(dimethylsiloxane) (PDMS) with two spacers. (b)–(e) Typical images of the contact region as the distance between the spacers ($2l$) is progressively increased: $2l = 14.5$, 19.5, 22.5, and 27.6 mm, respectively. These micrographs are obtained with a film of $\mu = 0.2$ MPa, $h = 40\,\mu$m, and a flexible plate of $D = 0.02$ Nm. (f) Amplitude data from experiments with films of shear modulus $\mu = 0.2 - 1.0$ MPa, thickness $h = 40 - 200\,\mu$m, and flexible plates of rigidity $D = 0.02 - 0.06$ Nm scaled as $\xi = Aq$ and plotted against the quantity h/c. The solid line is a guide to the eye. (g)–(h) These instability patterns can be generated on a partially crosslinked PDMS film, which can then be fully cross-linked to fix these patterns permanently. Typical atomic force microscopy images of such a permanently fixed pattern of the film ($\approx 150\,\mu$m) in close proximity to the fingers suggest that the maximum normal strain of the film is < 0.02. (g) Image of the region adjoining two fingers. (h) Tip of finger.

other, it is lifted off a film that is prestretched uniaxially. The confinement of the film increases in both of these experiments, with increase in the contact width and the extent of stretching.

EXPERIMENT WITH DOUBLE SPACERS

Materials

We obtained the glass slides (Corning microslides) and cover slips (Corning cover plates) from Fisher Scientific, USA. We cleaned the glass slides in a Harrick plasma cleaner (model PDC-23G, 100 W, Harrick Scientific, Pleasantville, NY, USA) before surface treatment. The material for film preperation, *i.e.*, vinyl-endcapped poly(dimethylsiloxane) oligomers of different chain lengths, platinum catalyst, and the methylhydrogen siloxane cross-linker, were obtained as gifts from Dow Corning Corp., Midland, MI, USA. We used also two sets of filler gauges of various thicknesses, which were purchased from a local auto-parts shop. The instability patterns were observed with a Nikon Diaphot (Nikon, USA) inverted microscope equipped with a charge coupled device (CCD) camera and a video recorder.

Method

Figure 1(a) depicts the schematic of the first experiment in which the flexible plate is detached from the bonded elastic layer by inserting two spacers of height Δ on two sides of the plate/film interface. The distance between the spacers is $2l$. The spacers generate two propagating cracks at the interface and peel the flexible plate off the adhesive film from both its ends. A finite contact width, $2c$, is attained following the equilibrium of forces, which include the adhesion and elastic forces in the adhesive and the adherent. When the spacers remain far apart, so that $2l$ and $2c$ both tend to infinity, the experiment represents the limiting case in which a single spacer is used to lift the flexible plate off the film from one of its ends [11]. However, as the distance $2l$ is decreased, the contact width $2c$ shrinks, thereby increasing the curvature of the plate. Finally, a distance is reached at which the stress required to bend the plate exceeds the adhesion strength of the interface and the plate no longer remains stuck to the film. Here we present a systematic analysis of this experiment to rationalize our experimental observations.

Preamble

Because no dynamics is involved in the formation of these unconditionally stable patterns, we develop our arguments on the premise that

their final states are attained by the minimization of the overall energy of the system. In particular, we consider four types of energy: the bending energy of the contacting plate, the elastic energy of the film, the adhesion energy at the interface of the plate and the film, and the surface energy associated with the creation of curved surface near the finger region. This last contribution however, is, negligible in comparison with the elastic energy of the film as the ratio of two scales [11] $\gamma/\mu h \approx 10^{-5}$ where γ is the surface energy of the film and μ is its shear modulus. Furthermore, following observations from experiments, the contacting plate has been assumed to bend only in the direction of propagation of the contact line (*i.e.*, along x), remaining uniform along the wave vector (*i.e.*, along y); its contribution to the total energy has been accounted for accordingly. Although, because of the peeling action on the plate, the film deforms normal to the surface, because of its own incompressibility, it sags in the vicinity of the contact line. For a thick film, the shear deformation occurs in both the xy and yz planes, *i.e.*, in planes normal to the z and the x axes, respectively. The latter deformation causes sagging in the region ahead of the line of contact of the film and the plate, which is enough to compensate for the normal deformation of the film. This kind of deformation does not cause undulation of the contact line. However, when the film is thin, the hydrostatic stress in it causes shear deformations also in the xz (*i.e.*, normal to y axes) plane. It is this additional lateral deformation that results in undulation of the contact line, which is accounted for in the energy calculations. The remaining component of the energy is the work of adhesion, which depends on the area of contact between the film and the cover plate. Previous studies [13] indicated that the magnitude of the adhesion energy does not affect the wavelength of the instability. These linear analyses, however, provide no information about the amplitude of the instability. In the current problem, as the overall energy is minimized with respect to wavelength and amplitude as variables, a weak nonlinearity is naturally invoked that presupposes a geometric and energetic relationship between these two variables. This nonlinearity is valuable in generating the bifurcation diagram of the morphology of fingers, in which the total energy goes through a minimum at specific amplitude and wavelength for a given confinement parameter. Our analysis shows that such minima exist only when the film is sufficiently confined.

Governing Equations and Boundary Conditions

In the absence of any body force, the stress and the displacement profiles in the elastic adhesive are obtained by solving the stress

equilibrium and the incompressibility relations for an incompressible elastic material:

$$-\overline{\nabla}p + \mu\nabla^2\bar{u} = 0 \qquad \text{and} \qquad \overline{\nabla}\cdot\bar{u} = 0 \tag{1}$$

where p is the pressure field and $\bar{u} = u\overline{e_x} + v\overline{e_y} + w\overline{e_z}$ is the displacement vector in the film with x, y, and z being, respectively, the direction of propagation of the contact line, the direction of the wave vector, and the thickness coordinate of the film. The $x = 0$ line, *i.e.*, the y axis, goes through the tip of the wavy contact line, whose position is represented by $\eta(y)$. Equations (1) are solved with the following boundary conditions [11–15]:

(a) The film remains perfectly bonded to the rigid substrate so that at $z = 0$, displacements $\bar{u} = 0$.

(b) The flexible contacting plates are coated with a self-assembled monolayer (SAM) of hexadecyltrichlorosilane molecules, which allow for partial slippage at the interface of the film and the flexible plate, *i.e.*, at $z = h + \psi$, where ψ is the vertical displacement of the interface measured from the undeformed surface of the film. Although similar surface treatments can alter the interfacial friction as evident in our earlier experiments [14,19], the wavelength of perturbations does not depend on the level of frictional resistance at the surface. Furthermore, our calculation in Ref. [18] shows that the two extreme conditions of perfect bonding and infinite slippage both lead to similar values for work of adhesion at the interface. Hence, for the sake of simplicity, we assume frictionless contact at the film–flexible plate interface so that the shear stress $\sigma_{xz}\big|_{z=h+\psi} = \sigma_{yz}\big|_{z=h+\psi} = 0$.

(c) At the film–flexible plate interface $(x < \eta(y))$, the traction on the film is equal to the bending stress on the plate, which, in our experiments, bends through a very small angle of less than 1°. Hence, under small bending approximations, we have $\sigma_{zz}\big|_{x<\eta(y),z=h+\psi} + D\Delta^2\psi = 0$, *i.e.*, $\left(-p + 2\mu\frac{\partial w}{\partial z}\right)\big|_{x<\eta(y),z=h+\psi} + D\Delta^2\psi = 0$. At $\eta(y) < x < a$, the film and the plate are free of any traction, so that $\sigma_{zz}\big|_{\eta(y)<x<a,z=h+\psi} = 0$ and $D\Delta^2\psi = 0$. Here a represents the distance of the spacer from $x = 0$. These boundary conditions applied at the two different regions then should lead to discontinuity of the normal stress across the contact line. However, this discontinuity does not occur, because within a very small distance away from the contact line $x > \eta(y)+$, the film and the plate remain subjected to distance-dependent intermolecular forces of adhesion, which drop continuously to zero, leading to a continuous variation of the normal stress. This point is further elaborated in the following paragraph.

(d) Although there is no ambiguity regarding this set of boundary conditions applied in the two regions, *i.e.*, at $x < \eta(y)$ and at

$\eta(y) < x < a$, the nature of the boundary condition at $x = \eta(y)$ is less clear and has been a subject of considerable discussions in recent years [20–22]. Recently, Adda-Bedia and Mahadevan [23] treated the crack-tip instability problem by considering a single plate in contact with a thin, soft, elastic film. At the boundary line, they considered the condition of the classical singularity of normal stress, which led to the discontinuity of the displacement derivatives of the plate and the film. However, Maugis [20], who discussed this issue rather extensively, came to the conclusion that singularity of the stress field, as developed by the remote loading at the crack-tip, is cancelled by another singularity due to internal loading resulting from the cohesive stresses at the crack-tip. The cancellation of the two singularities leads to a smooth variation of all the slopes at the crack-tip region. The problem has also been addressed recently [20,22] from the point of view that the stress at the crack-tip for soft polymer films cannot exceed the value of its elastic modulus because the polymer chains bridging the two surfaces undergo thermal fluctuations. While Ref. [21] treats the problem using rigorous statistical mechanics, here we address the problem in a somewhat simplified way by considering that any one of the bridging chains can be either in the attached or detached state. At equilibrium, the areal density of the bonded chains is given by

$$\Sigma_b = \frac{\Sigma_0}{1 + \exp(k_s\delta^2/2k_BT - \varepsilon_A/k_BT)} \tag{2}$$

where Σ_0 is the total areal density of bonded and unbonded chains, k_s is the spring constant of the chain, ε_A is the energy of adsorption per chain, and δ is the extension of the chain. The stress is obtained by multiplying Σ_b by the spring force $(k_s\delta)$. Furthermore, recognizing that the spring constant (k_s) of a Gaussian chain is given by $k_BT/n_sl_s^2$ (l_s is the statistical segment length and n_s is the numbers of statistical segments per chain) and the elastic modulus of the network $E \approx k_BT/n_sl_s^3$, the normal stress at the interface can be written as

$$\sigma = \frac{E\sqrt{2\phi/k_BT}}{1 + \exp(\phi - \varepsilon_A/k_BT)} \tag{3}$$

where $\phi = k_s\delta^2/2$. This representation suggests that the normal stress, σ, converges asymptotically to zero for ϕ approaching either zero or infinity and attains a maximum at an intermediate value of ϕ. Far away from the crack-tip, *i.e.*, at $x \to -\infty$, at the interface of the film and the plate, no polymer chain is stretched so that the normal stress is zero. Within the cohesive zone of the crack-tip, as we traverse in the other direction, the polymer chains get more and more stretched, thus

ϕ increases. However, this increase in ϕ is accompanied by the decrease in number of the bonded chains, resulting in the decrease of the normal stress as dictated by Eq. (2). Within these two zones, in the open mouth of the crack, very close to the crack-tip, *i.e.*, at $x \to \eta(y)$, the normal stress, σ, goes through a maximum. However, this stress cannot exceed the maximum cohesive stress at the contact line, which is only a fraction of the elastic modulus, E, as predicted by Eq. (3) for representative values of the adsorption energy, ε_A, for van der Waals interactions. For these soft materials, therefore, the normal stress rises smoothly to a finite maximum value at the crack-tip and then it falls smoothly within a very small distance of the contact line. Within the context of the continuum mechanics formalism, we use the boundary condition that the hydrostatic tension is maximum in the near vicinity of the contact line, *i.e.*, $\frac{\partial p}{\partial x}\big|_{x=\eta(y)} = 0$.

Using this boundary conditions, we proceed to solve Eq. (1). We first write the displacements and the coordinates in dimensionless form using the following two length scales: $q^{-1} = (Dh^3/3\mu)^{1/6}$ as the characteristic length along x obtained naturally from the analysis presented in Refs. [14] and [15] and the thickness, h, of the film as that along y following observation that the wavelength of instability, λ, varies linearly with the thickness of the film [11]. Furthermore, thickness, h, is also the characteristic length along the z axis. Using these characteristic lengths, we obtain the following dimensionless quantities:

$$X = xq, \qquad Y = \frac{y}{h}, \qquad Z = \frac{z}{h}, \qquad U = uq, \qquad V = \frac{v}{h}, \qquad W = \frac{w}{h}.$$

We write the stresses also in dimensionless form by dividing them by μ/ε^2 as the characteristic pressure

$$P = \frac{p}{(\mu/\varepsilon^2)}, \qquad \Sigma_{XZ} = \frac{\sigma_{XZ}}{(\mu/\varepsilon^2)}, \qquad \Sigma_{YZ} = \frac{\sigma_{YZ}}{(\mu/\varepsilon^2)}.$$

Using these dimensionless quantities, the stress equilibrium and incompressibility relations are written as

$$\frac{\partial P}{\partial X} = \varepsilon^2 \frac{\partial^2 U}{\partial X^2} + \frac{\partial^2 U}{\partial Y^2} + \frac{\partial^2 U}{\partial Z^2}, \qquad \frac{\partial P}{\partial Y} = \varepsilon^4 \frac{\partial^2 V}{\partial X^2} + \varepsilon^2 \left(\frac{\partial^2 V}{\partial Y^2} + \frac{\partial^2 V}{\partial Z^2} \right),$$
$$\frac{\partial P}{\partial Z} = \varepsilon^4 \frac{\partial^2 W}{\partial X^2} + \varepsilon^2 \left(\frac{\partial^2 W}{\partial Y^2} + \frac{\partial^2 W}{\partial Z^2} \right), \tag{4}$$

and

$$\frac{\partial U}{\partial X} + \frac{\partial V}{\partial Y} + \frac{\partial W}{\partial Z} = 0,$$

and the boundary conditions result in

$$
\begin{aligned}
&\text{(a) } U(Z=0) = V(Z=0) = 0,\\
&\text{(b) } \Sigma_{XZ}(X,Y,Z=1+\Psi) = 0 = \Sigma_{YZ}(X,Y,Z=1+\Psi),\\
&\qquad \text{or } \left(\frac{\partial U}{\partial Z} + \varepsilon^2 \frac{\partial W}{\partial X}\right) = \left(\frac{\partial V}{\partial Z} + \frac{\partial W}{\partial Y}\right) = 0,\\
&\text{(c) } P(Z=1+\Psi) = 2\varepsilon^2 \frac{\partial W}{\partial Z}\bigg|_{Z=1+\Psi} + 3\left(\frac{\partial^4 \Psi}{\partial X^4} + \frac{2}{\varepsilon^2}\frac{\partial^4 \Psi}{\partial X^2 \partial Y^2} + \frac{1}{\varepsilon^4}\frac{\partial^4 \Psi}{\partial Y^4}\right) \qquad (5)\\
&\qquad \text{at } X < \mathrm{N}(Y),\\
&\text{(d) } 0 = \frac{\partial^4 \Psi}{\partial X^4} \qquad \text{at } \mathrm{N}(Y) < X < aq,\\
&\text{(e) } \frac{\partial P}{\partial X}\bigg|_{X=\mathrm{N}(Y)} = 0,
\end{aligned}
$$

where aq is the dimensionless distance of the spacer from $X = 0$, Ψ is the dimensionless vertical displacement of plate, and $X = \mathrm{N}(Y)$ represents the position of the contact line in the dimensionless form. We assume that the solutions of displacements and pressure consist of two components: the base solutions, which vary only along the X and Z axes and remain uniform along Y, and a perturbation term, which appears over and above these base solutions and incorporates the spatial variation of the displacements along the y axis. The general form of these solutions are expressed as [24] $T = T_0(X,Z) + \varepsilon^2 T_1(X,Y,Z) + \varepsilon^4 T_2(X,Y,Z) + \ldots$, where $T = P, U, V,$ and W. Similarly, the vertical displacement, Ψ, of the plate is expanded as $\Psi = \Psi_0(X) + \varepsilon^2 \Psi_1(X,Y) + \varepsilon^4 \Psi_2(X,Y) + \ldots$. Here, the base solutions are of order ε^0, and the perturbed ones are of order $\varepsilon^2, \varepsilon^4$, etc. At this juncture, it is worthwhile to point out the physical nature of the perturbation as ε^2 approaches zero, which corresponds to the stress decay length, q^{-1}, approaching infinity. For any finite deformation of the elastomeric film at the crack-tip region, the condition implies that the local radius of curvature of the cantilever plate also approaches infinity or that the slope of the cantilever plate is vanishingly small. As we show, this base state solution follows from the premise that the pressure and the displacements remain uniform along the y axis, and the classical lubrication approximation is applicable. Later, we seek a solution of Eq. (4) {or Eq. (6)} by considering periodic perturbations of the field variables along the y direction. This leads to a geometric perturbation of the contact line, where the base state corresponds to a vanishing wave vector of the periodic perturbation (*i.e.*, straight contact line).

Notice that in a typical experiment $h = 50\,\mu\text{m}$, $\mu = 1.0\,\text{MPa}$, and $D = 0.02\,\text{Nm}$, so that $\varepsilon^2 = 0.03 \ll 1$ is small enough to allow perturbation expansion for the displacement and pressure fields as powers of ε^2. When we insert these definitions in Eq. (4) and separate the base (Y independent) and the perturbation (Y dependent) terms, we obtain

$$\begin{aligned} -\frac{\partial P_0}{\partial X} + \varepsilon^2\frac{\partial^2 U_0}{\partial X^2} + \frac{\partial^2 U_0}{\partial Z^2} = \varepsilon^4\frac{\partial^2 V_0}{\partial X^2} + \varepsilon^2\frac{\partial^2 V_0}{\partial Z^2} = 0, \\ -\frac{\partial P_0}{\partial Z} + \varepsilon^4\frac{\partial^2 W_0}{\partial X^2} + \varepsilon^2\frac{\partial^2 W_0}{\partial Z^2} = \frac{\partial U_0}{\partial X} + \frac{\partial W_0}{\partial Z} = 0, \end{aligned} \tag{6}$$

and

$$\begin{aligned} \varepsilon^2\frac{\partial P_1}{\partial X} + \varepsilon^4\frac{\partial P_2}{\partial X} &= \varepsilon^2\left(\frac{\partial^2 U_1}{\partial Y^2} + \frac{\partial^2 U_1}{\partial Z^2}\right) \\ &\quad + \varepsilon^4\left(\frac{\partial^2 U_1}{\partial X^2} + \frac{\partial^2 U_2}{\partial Y^2} + \frac{\partial^2 U_2}{\partial Z^2}\right) + \varepsilon^6\frac{\partial^2 U_2}{\partial X^2}, \\ \varepsilon^2\frac{\partial P_1}{\partial Y} + \varepsilon^4\frac{\partial P_2}{\partial Y} &= \varepsilon^4\left(\frac{\partial^2 V_1}{\partial Y^2} + \frac{\partial^2 V_1}{\partial Z^2}\right) + \varepsilon^6\left(\frac{\partial^2 V_1}{\partial X^2} + \frac{\partial^2 V_2}{\partial Y^2} + \frac{\partial^2 V_2}{\partial Z^2}\right), \\ \varepsilon^2\frac{\partial P_1}{\partial Z} + \varepsilon^4\frac{\partial P_2}{\partial Z} &= \varepsilon^4\left(\frac{\partial^2 W_1}{\partial Y^2} + \frac{\partial^2 W_1}{\partial Z^2}\right) + \varepsilon^6\left(\frac{\partial^2 W_1}{\partial X^2} + \frac{\partial^2 W_2}{\partial Y^2} + \frac{\partial^2 W_2}{\partial Z^2}\right), \\ 0 &= \frac{\partial U_1}{\partial X} + \frac{\partial V_1}{\partial Y} + \frac{\partial W_1}{\partial Z}, \end{aligned} \tag{7}$$

which are solved using the following boundary conditions derived from Eqs. (5a–e):

(a) at $Z = 0$,

$U_0 = W_0 = 0$ and $\varepsilon^2 U_1 + \varepsilon^4 U_2 = \varepsilon^2 V_1 + \varepsilon^4 V_2 = \varepsilon^2 W_1 + \varepsilon^4 W_2 = 0$;

(b) at $Z = 1 + \Psi$,

$$\frac{\partial U_0}{\partial Z} + \varepsilon^2\frac{\partial W_0}{\partial X} = \frac{\partial W_0}{\partial Y} = 0 \quad \text{and}$$

$$\varepsilon^2\frac{\partial U_1}{\partial Z} + \varepsilon^4\left(\frac{\partial U_2}{\partial Z} + \frac{\partial W_1}{\partial X}\right) = \varepsilon^2\left(\frac{\partial V_1}{\partial Z} + \frac{\partial W_1}{\partial Y}\right) + \varepsilon^4\left(\frac{\partial V_2}{\partial Z} + \frac{\partial W_2}{\partial Y}\right) = 0;$$

(c) at $Z = 1 + \Psi$,

$$P_0 = 3\frac{\partial^4 \Psi_0}{\partial X^4} + 2\varepsilon^2\frac{\partial W_0}{\partial Z}, \qquad X < 0,$$

$$\varepsilon^2 P_1 + \varepsilon^4 P_2 = \frac{1}{\varepsilon^2}\frac{\partial^4 \Psi_1}{\partial Y^4} + \left(2\frac{\partial^4 \Psi_1}{\partial X^2 \partial Y^2} + \frac{\partial^4 \Psi_2}{\partial Y^4}\right),$$

and

$$X < \mathrm{N}(Y) + \varepsilon^2\left(3\frac{\partial^4\Psi_1}{\partial X^4} + 2\frac{\partial^4\Psi_2}{\partial X^2\partial Y^2}\right) + \varepsilon^4\left(3\frac{\partial^4\Psi_2}{\partial X^4} + 2\frac{\partial W_1}{\partial Z}\right);$$

(d) at $Z = 1 + \Psi$,

$$0 = \frac{\partial^4\Psi_0}{\partial X^4}, \qquad 0 < X < aq,$$

and

$$0 = \varepsilon^2\frac{\partial^4\Psi_1}{\partial X^4} + \varepsilon^4\frac{\partial^4\Psi_2}{\partial X^4}, \qquad \mathrm{N}(Y) < X < aq,$$

$$\text{(e) } 0 = \left.\frac{\partial P_0}{\partial X}\right|_{X=0} \quad \text{and} \quad 0 = \varepsilon^2\left.\frac{\partial P_1}{\partial X}\right|_{X=\mathrm{N}(Y)} + \varepsilon^4\left.\frac{\partial P_2}{\partial X}\right|_{X=\mathrm{N}(Y)}. \tag{8}$$

Solution of Eq. (6) using Long Scale Approximation

We solve Eq. (6) in light of boundary conditions in Eq. (8). However, the characteristic length scales along x and z axes are so far apart that $\varepsilon^2 << 1$, as noted earlier. This allows us to simplify these equations using the long-scale approximations [21]:

$$-\frac{\partial P_0}{\partial X} + \frac{\partial^2 U_0}{\partial Z^2} = -\frac{\partial P_0}{\partial Z} = \frac{\partial U_0}{\partial X} + \frac{\partial W_0}{\partial Z} = 0;$$

at $Z = 0,\ U_0 = W_0 = 0$, and at $Z = 1 + \Psi$,

$$\frac{\partial U_0}{\partial Z} = \frac{\partial W_0}{\partial Y} = 0.$$

When these equations are integrated over $0 < Z < 1 + \Psi_0$, the following relations for the displacements in the film are obtained:

$$\begin{aligned} U_0 &= \frac{\partial P_0}{\partial X}\left(\frac{Z^2}{2} - (1+\Psi_0)Z\right), \\ W_0 &= -\frac{\partial^2 P_0}{\partial X^2}\frac{Z^3}{6} + \frac{Z^2}{2}\left(\frac{\partial^2 P_0}{\partial X^2}(1+\Psi_0) + \frac{\partial P_0}{\partial X}\Psi_0\right). \end{aligned} \tag{9}$$

Hence, the vertical displacement $\Psi_0 = W_0|_{Z=1+\Psi_0}$ of the interface is obtained as

$$\begin{aligned} \Psi_0 &= \frac{\partial^2 P_0}{\partial X^2}\frac{(1+\Psi_0)^3}{3} + \frac{\partial P_0}{\partial X}\frac{\Psi_0(1+\Psi_0)^2}{2}, \\ &= \frac{\partial^6\Psi_0}{\partial X^6}(1+\Psi_0)^3 + \frac{\partial^5\Psi_0}{\partial X^5}\frac{3\Psi_0(1+\Psi_0)^2}{2}. \end{aligned} \tag{10}$$

Although the nonlinearity of this equation renders it nonamenable to analytical solutions, we simplify it by noting that in all our experiments the dimensionless vertical displacement $\Psi_0 < 0.02$. Thus, linearization of the equation results in

$$\Psi_0 - \frac{\partial^6 \Psi_0}{\partial X^6} = 0 \qquad \text{at } X < 0. \tag{11}$$

At $0 < X < aq$, there is no traction on the plate, *i.e.*, $\partial^4 \Psi_0 / \partial x^4 = 0$. Equation (11) is solved using the boundary condition that about the centerline $X = -cq$ of the contact area, displacement Ψ_0 and the bending moment and normal stress on plate are continuous, so that

$$\frac{\partial \Psi_0}{\partial X} = \frac{\partial^3 \Psi_0}{\partial X^3} = \frac{\partial^5 \Psi_0}{\partial X^5} = 0$$

and that it is freely supported at $X = aq$ by the spacer

$$\left(\Psi_0|_{X=aq} = \overline{\Delta} = \frac{\Delta}{h}, \quad \frac{\partial^2 \Psi_0}{\partial X^2} = 0 \right).$$

Finally, at the vicinity of the contact line ($X = 0$) displacement, slope, bending moment, and vertical shear force are continuous, so that

$$\Psi_0|_{X=0-} = \Psi_0|_{X=0+}, \left.\frac{\partial \Psi_0}{\partial X}\right|_{X=0-} = \left.\frac{\partial \Psi_0}{\partial X}\right|_{X=0+}, \left.\frac{\partial^2 \Psi_0}{\partial X^2}\right|_{X=0-} = \left.\frac{\partial^2 \Psi_0}{\partial X^2}\right|_{X=0+}$$

and

$$\left.\frac{\partial^3 \Psi_0}{\partial X^3}\right|_{X=0-} = \left.\frac{\partial^3 \Psi_0}{\partial X^3}\right|_{X=0+}.$$

Maximal tensile stress at the contact line results in

$$\left.\frac{\partial P_0}{\partial X}\right|_{X=0} = \left.\frac{\partial^5 \Psi_0}{\partial X^5}\right|_{X=0} = 0.$$

In Fig. 2a and b, we plot the numerical solutions of dimensionless vertical displacement, Ψ_0, and normal stress $\Sigma_{0_{ZZ}} = \varepsilon^2 \sigma_{0_{zz}} / \mu$ ($\Sigma_{0_{ZZ}}$: base components of the normal stress on film) with respect to the dimensionless distance X for a representative set of values for dimensionless distances $aq = 15 - 25$ and $cq = 2.5 - 10$. Curve 1 represents the limiting case of semi-infinite contact area, for which the displacement and stress profiles remain oscillatory with exponentially diminishing amplitude away from the contact line [18], whereas curve 2 represents an intermediate situation in which contact area decreases as the

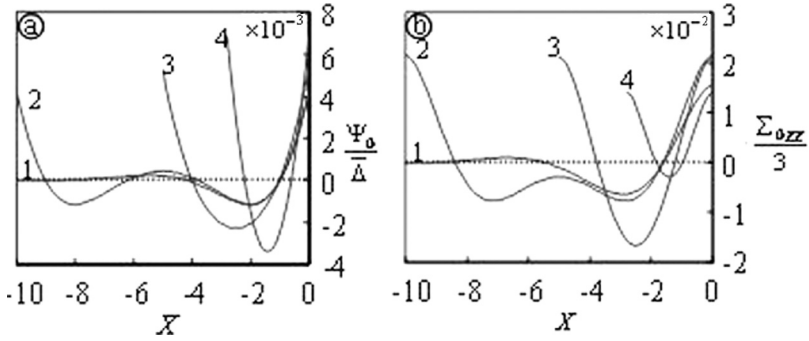

FIGURE 2 Plots depict the dimensionless vertical displacement, $\Psi_0/\overline{\Delta}$, and normal stress, $\Sigma_{0\,ZZ}/3$, in the elastic (PDMS) film in experiments of Fig. 1(a). The profile 1 obtained with interspacer distance $2l \to \infty$ represents the limiting case in which a single spacer peels off the plate. Curves 2–4, corresponding to $(aq = 25, cq = 5)$, $(15, 2.5)$ and $(15, 1.4)$ are obtained when $2l$ is progressively reduced, thereby decreasing the width of the contact area.

spacers are brought closer. Here, too, we see oscillatory profiles with diminishing amplitude, but the number of oscillation decreases. Finally, for curves 3 and 4, the contact width is so small that a region of positive Ψ_0 and $\Sigma_{0_{ZZ}}$ close to $X = 0$ is followed by a region of negative values of Ψ_0 and $\Sigma_{0_{ZZ}}$. Using the expressions of these displacement profiles, we can estimate the total energy of the system, which consists of the elastic energy of the film, the bending energy of the plate, and the interfacial work of adhesion, W_A. The dimensionless form of the total energy is obtained as

$$\Pi_0 = \frac{\varepsilon^3}{2}\left(\int_{-cq}^{aq}\left(\frac{d^2\Psi_0}{dX^2}\right)^2 dX + \frac{1}{6}\int_{-cq}^{aq}\int_0^1\left(\frac{\partial U_0}{\partial Z} + \varepsilon^2\frac{\partial W_0}{\partial X}\right)^2 dX dZ\right) + \frac{W_A h^2}{D}\frac{aq}{\varepsilon}, \tag{12}$$

which is a function of the four dimensionless quantities $aq, \varepsilon, W_A h^2/D$, and cq, the numerical value of which are such that the total energy of the system is minimum. This latter condition allows us to obtain one of the parameters for a given set of three other parameters. For example, for a given set of values of cq, ε, and $W_A h^2/D$, we obtain aq by minimizing

$$\Pi_0 : \left.\frac{\partial \Pi_0}{\partial (aq)}\right|_{cq,\varepsilon,W_A h^2/D} = 0.$$

It is important to note also that in curves 1 and 2 of Figs. 2a and b, normal and shear stresses remain concentrated within a distance equivalent to one wavelength of the oscillation, *i.e.*, $\approx 5q^{-1}$; for curves 3 and 4, this distance spans to half the width of the contact area, *i.e.*, c. Therefore, for these profiles, the relevant characteristic length along x is not q^{-1} but c, which motivates us to redefine the confinement parameter as h/c.

Geometric Perturbation Analysis

We now discuss the situation when the contact line becomes undulatory. The effect of confinement on the contact line instability is evident in the video-micrographs 1b–e, which show the typical images of the contact region with increasing contact width $2c$. No undulation can be observed when the distance $2c$ decreases to less than a critical value; however, they appear along the contact line when the contact width is increased and their amplitude progressively increases with further increase in $2c$. We measure the amplitude, A, of these waves, after the contact line stops completely and normalize it as $\xi = Aq$. These data summarized in Fig. 1f show that the scaled amplitude, ξ, varies inversely with the confinement parameter, h/c. The amplitude, however, does not increase from zero but from a finite value at the critical confinement, $h/c = 0.14$. No undulations could be observed beyond this limit.

To estimate the threshold confinement at which nontrivial solutions of excess quantities $(T_i, i \neq 0)$ are energetically favorable, we solve the following equations obtained by matching the coefficients for $\varepsilon^i,\ i = 2, 4$ in the left- and the right-hand side of Eq. (7):

$$
\begin{aligned}
&\text{(a) } \varepsilon^2 : \frac{\partial P_1}{\partial X} = \frac{\partial^2 U_1}{\partial Y^2} + \frac{\partial^2 U_1}{\partial Z^2}, \qquad \frac{\partial P_1}{\partial Y} = 0, \qquad \frac{\partial P_1}{\partial Z} = 0;\\
&\text{(b) } \varepsilon^4 : \frac{\partial P_2}{\partial X} = \frac{\partial^2 U_1}{\partial X^2} + \frac{\partial^2 U_2}{\partial Y^2} + \frac{\partial^2 U_2}{\partial Z^2}, \qquad \frac{\partial P_2}{\partial Y} = \frac{\partial^2 V_1}{\partial Y^2} + \frac{\partial^2 V_1}{\partial Z^2},\\
&\qquad \frac{\partial P_2}{\partial Z} = \frac{\partial^2 W_1}{\partial Y^2} + \frac{\partial^2 W_1}{\partial Z^2};\\
&\text{(c) } \frac{\partial U_1}{\partial X} + \frac{\partial V_1}{\partial Y} + \frac{\partial W_1}{\partial Z} = 0.
\end{aligned}
\tag{13}
$$

Similarly, the boundary conditions in Eq. (8) result in

(a) at $Z = 0$,

$$\varepsilon^2 : U_1 = V_1 = W_1 = 0, \quad \varepsilon^4 : U_2 = V_2 = W_2 = 0;$$

(b) at $Z = 1 + \Psi$,

$$\varepsilon^2 : \frac{\partial U_1}{\partial Z} = \left(\frac{\partial V_1}{\partial Z} + \frac{\partial W_1}{\partial Y}\right) = 0, \quad \varepsilon^4 : \frac{\partial U_2}{\partial Z} + \frac{\partial W_1}{\partial X} = \frac{\partial V_2}{\partial Z} + \frac{\partial W_2}{\partial Y} = 0;$$

(c) at $Z = 1 + \Psi$ and $X < \mathrm{N}(Y)$,

$$\varepsilon^{-2} : 0 = \frac{\partial^4 \Psi_1}{\partial Y^4},$$

$$\varepsilon^{0} : 0 = 2\frac{\partial^4 \Psi_1}{\partial X^2 \partial Y^2} + \frac{\partial^4 \Psi_2}{\partial Y^4},$$

$$\varepsilon^{2} : P_1 = 3\frac{\partial^4 \Psi_1}{\partial X^4} + 2\frac{\partial^4 \Psi_2}{\partial X^2 \partial Y^2};$$

(d) at $Z = 1 + \Psi$ and $N(Y) < X < aq$,

$$\varepsilon^{2} : 0 = \frac{\partial^4 \Psi_1}{\partial X^4} \tag{14}$$

We further assume that the excess displacements and pressure vary sinusoidally along $Y : T_i = \overline{T}_i \sin(KY)$; $T = U, W$ and P; and $V_i = \overline{V}_i \cos(KY)$: $i = 1,2, \ldots$, where $K = 2\pi/(\lambda/h)$ is the dimensionless wave number of the perturbed waves and λ is the wavelength. Notice that the long-scale approximations used for estimating the nonperturbative (*i.e.*, when the contact line is not undulatory) solutions are not relevant for obtaining the expressions for the perturbed components, because, here, the simplification is effected by mapping the coefficients of ε^i, $i = 2, 4$ on either side of the Eq. (7). Using these new definitions for the excess quantities in Eq. (13), we obtain the following equations:

$$\begin{aligned}
&\text{(a) } \varepsilon^2 : \frac{d\overline{P_1}}{dX} = -K^2\overline{U_1} + \frac{d^2\overline{U_1}}{dZ^2}, \qquad \overline{P_1} = 0, \qquad \frac{d\overline{P_1}}{dZ} = 0;\\
&\text{(b) } \varepsilon^4 : \frac{d\overline{P_2}}{dX} = \frac{d^2\overline{U_1}}{dX^2} - K^2\overline{U_2} + \frac{d^2\overline{U_2}}{dZ^2}, \qquad K\overline{P_2} = -K^2\overline{V_1} + \frac{d^2\overline{V_1}}{dZ^2},\\
&\qquad \frac{d\overline{P_2}}{dZ} = -K^2\overline{W_1} + \frac{d^2\overline{W_1}}{dZ^2};\\
&\text{(c) } \frac{d\overline{U_1}}{dX} - K\overline{V_1} + \frac{d\overline{W_1}}{dZ} = 0;
\end{aligned} \tag{15}$$

which are solved using the following boundary conditions obtained from Eqs. (14a and b):

(a) at $Z = 0$,

$$\varepsilon^2 : \overline{U_1} = \overline{V_1} = \overline{W_1} = 0, \qquad \varepsilon^4 : \overline{U_2} = \overline{V_2} = \overline{W_2} = 0;$$

(b) at $Z = 1 + \Psi$,

$$\varepsilon^2 : \frac{d\overline{U_1}}{dZ} = \left(\frac{d\overline{V_1}}{dZ} + K\overline{W}_1\right) = 0,$$

$$\varepsilon^4 : \frac{d\overline{U_2}}{dZ} + \frac{d\overline{W}_1}{dX} = \frac{d\overline{V}_2}{dZ} + K\overline{W}_2 = 0. \tag{16}$$

Equation (15a) suggests that the ε^2 order of the excess pressure, P_1, is zero, whereas that for the ε^4 order of the pressure, P_2, is finite, implying that the film undergoes undulations at the surface under a very small excess pressure. This excess pressure, however small, varies along Y, signifying that it depends upon the gap between the plate and film [13,25]. Nevertheless, this excess pressure applies only in the immediate vicinity ($< 0.1\mu$m) of the contact between the film and plate as the gap between the two increases rather sharply, as can be seen in the atomic force microscope (AFM) images presented in Fig. 1 g; it does not contribute significantly to the overall energy of the final state of the system. Therefore, in this calculation, we find only the ε^2 order of the excess displacements and pressure. These are obtained by solving Eq. (15) subjected to the boundary conditions in (16a–b) relevant to the film; as for the plate, its excess vertical displacement is such that it remains in contact with the film only through one-half of the wave. Hence, a simple way of expressing the excess displacement of the plate is $\Psi_1 = \overline{W}_1(X, Z = 1 + \Psi) + \Psi_{11}(X)\ (1 - \sin(KY))$ and $\Psi_2 = \overline{W}_2(X, Z = 1 + \Psi) + \Psi_{22}(X)(1 - \sin(KY))$, in which Ψ_{11} and Ψ_{22} are the amplitudes. This definition implies that the plate remains in contact with the film at $KY = (2n + 1)\pi/2$, $n = 0, 2, 4, \ldots$. At all other values of KY, it remains out of contact. Notice that this definition ensures only a line contact between the plate and the film; this has to do with the fact that here we consider only one component of the Fourier spectrum. A more accurate approach would be to consider all the components, which would ensure contact through one-half of the wave as was done rather elegantly by Sarkar *et al.* [25] while modeling the debonding of a rigid plate from a confined elastic layer bonded to a rigid substrate. However, at the onset of appearance of the perturbation, it is sufficient to consider only a single wave vector of the whole spectrum to obtain the condition of occurrence of the instability. We assume further that $\Psi_{11} \ll \overline{W}_1$ and $\Psi_{22} \ll \overline{W}_2$, so that we can write directly $\Psi_1 = \overline{W}_1(X, Z = 1 + \Psi)$ and $\Psi_2 = \overline{W}_2(X, Z = 1 + \Psi)$ without sacrificing much accuracy. In essence, this assumption implies that the plate bends only along the X axis, remaining uniform along Y, as we observed in our experiments. Then the boundary conditions (14c) and (14d) simplify to the following equations for the excess displacement of the plate: at $Z = 1 + \Psi,\ X < \mathrm{N}(Y)$,

$$0 = \frac{\partial^4 \Psi_1}{\partial X^4};$$

at $\mathrm{N}(Y) < X < aq$,

$$0 = \frac{\partial^4 \Psi_1}{\partial X^4}. \tag{17}$$

In essence, this condition is applicable at any X; then it is convenient to apply the following boundary conditions at $X = 0$, rather than at $X = \mathrm{N}(Y)$:

The excess displacement, Ψ_1, and its slope are continuous at $X = 0$ so that

$$\Psi_1|_{X=0-} = \Psi_1|_{X=0+} = C_0\Phi(K), \qquad \left.\frac{\partial\Psi_1}{\partial X}\right|_{X=0-} = \left.\frac{\partial\Psi_1}{\partial X}\right|_{X=0+},$$

$$\text{and } \left.\frac{\partial^2\Psi_1}{\partial X^2}\right|_{X=0-} = \left.\frac{\partial^2\Psi_1}{\partial X^2}\right|_{X=0+}.$$

.

Here, $C_0\Phi(K)$ is the excess stretching of the film at $X = 0$ (Ref. 13), C_0 is a constant, and the function $\Phi(K)$ falls out naturally from the solution of the excess quantities. At $X = -\xi$, where, $\xi = Aq$ is the dimensionless amplitude of the waves the excess displacement of the plate, its slope vanishes, which results in the boundary condition:

$$\Psi_1|_{X=-\xi} = \left.\frac{\partial\Psi_1}{\partial X}\right|_{X=-\xi} = 0.$$

Similarly, at $X = aq$, excess displacement and curvature of the plate is zero, which results in the boundary condition

$$\Psi_1|_{X=aq} = \left.\frac{\partial^2\Psi_1}{\partial X^2}\right|_{X=aq} = 0.$$

Equation (15), and the boundary conditions discussed thus far, dictate the analytical expressions of the excess quantities which are the same as those obtained for the experiment with a single spacer and have been solved in Ref. 16.

Excess Energy

After obtaining the expressions for the base and the excess displacements [16], we proceed to estimate the excess energy of the system $\Pi = \Pi_{Total} - \Pi_0$. Using μ/ε^3 as the characteristic energy and considering only the leading order terms (ε^4 and ε^6), we obtain the expression for the excess energy as

$$\Pi = \frac{\varepsilon^6}{4}\int_{-\xi}^{0}\int_{0}^{2\pi/K}\int_{0}^{1}\left(\frac{\partial V_1}{\partial Z} + \frac{\partial W_1}{\partial Y}\right)^2 dZ\, dY\, dX + \frac{3\pi}{K}\int_{-\xi}^{aq}\left(2\varepsilon^2\frac{\partial^2\Psi_0}{\partial X^2}\frac{\partial^2\Psi_1}{\partial X^2} + \varepsilon^4\left(\frac{\partial^2\Psi_1}{\partial X^2}\right)^2\right)dX + \frac{6\xi}{K}\frac{W_A h^2}{D\varepsilon^4}. \qquad (18)$$

The first term in the right side corresponds to the excess elastic energy of the film, estimated only within a distance $-\xi \leq X \leq 0$, at which the surface of the film becomes undulatory. The second term corresponds to the bending energy of the plate, which needs to be estimated within a distance $-\xi \leq X \leq aq$. The third term represents the excess interfacial energy associated with the planar area of the fingers. We have neglected, however, the interfacial energy associated with their side walls.

After substituting the expressions for the base component of displacement Ψ_0 and the excess displacements V_1, W_1, and Ψ_1, we finally obtain

$$\Pi = (\varepsilon^6 f_2(\xi, cq, K) + \varepsilon^4 f_1(\xi, cq, K))C_0^2 + \varepsilon^2 f_3(\xi, cq, K)\overline{\Delta}C_0 + \frac{6\xi}{K}\frac{W_A h^2}{D\varepsilon^4}. \tag{19}$$

Here, the expressions for $f_1(\xi, cq, K), f_2(\xi, cq, K)$, and $f_3(\xi, cq, K)$ are obtained using Mathematica. Furthermore, hypothesizing that Π minimizes when $\partial\Pi/\partial C_0 = 0$, we obtain an expression for C_0, which, when substituted in Eq. (19), yields

$$\Pi = -\frac{\overline{\Delta}^2}{4}\frac{f_3^2}{f_1 + \varepsilon^2 f_2} + \frac{6\xi}{K}\frac{W_A h^2}{D\varepsilon^4}. \tag{20}$$

Thus, the excess energy, Π, is obtained as a function of three types of parameters: the length scales of perturbation (*i.e.*, wavelength λ/h and amplitude $\xi = Aq$), geometric length scales of the experiment (*i.e.*, h/c and ε), and dimensionless work of adhesion (*i.e.*, $W_A h^2/D$). Figure 3a depicts the dimensionless excess energy as a function of the dimensionless wave number, $K = 2\pi h/\lambda$, and amplitude, ξ, while h/c, ε, and $W_A h^2/D$ are kept constant. Π goes through a minimum ($\Pi_{\min}$), which remains positive as long as h/c is greater than a critical value. However, when $h/c < (h/c)_e$, we obtain a negative minimum for $\Pi_{\min}$, implying that undulations with finite amplitude are energetically favorable at and beyond this confinement. The corresponding values of λ/h, plotted against h/c in Figure 3b for a representative set of values of $\varepsilon = 0.19 - 0.35$ and $(W_A h^2/D)^{1/4} = 0.01 - 0.015$, show that undulations appear only when the film is sufficiently confined, *i.e.*, $h/c < 0.13$ as is observed in experiments (Figure 1f) with a variety of films of different thickness and modulus and cover plates of different rigidity. The wavelength of instability varies nonmonotonically with the contact width, which qualitatively captures the experimental observation that λ/h does not show monotonic increase or decrease with h/c as shown in Figure 3b. Furthermore, in the limit $h/c \to 0$, *i.e.*, for large enough

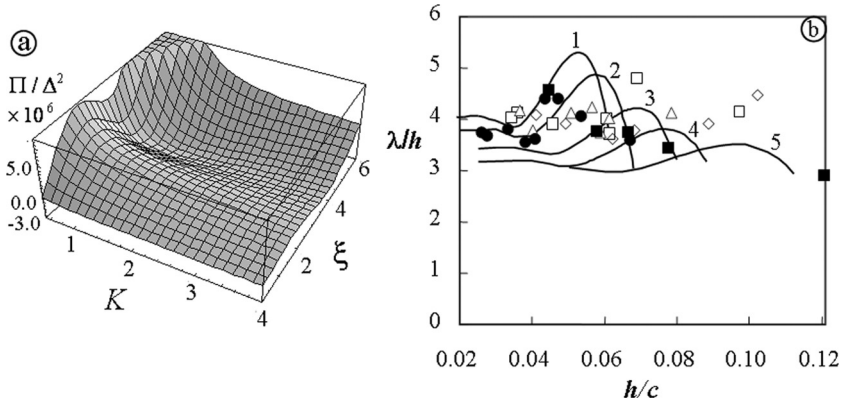

FIGURE 3 (a) Typical plot of dimensionless excess energy, Π, as a function of wavenumber $K = 2\pi h/\lambda$ and amplitude $\xi = Aq$ of fingers for dimensionless parameters: $\varepsilon = 0.29$, $h/c = 0.084$, and $(W_A h^2/D)^{1/4} = 0.008$. Instability ensues when Π is negative and minimum. (b) These plots are obtained for variety of ε and h/c at a given $(W_A h^2/D)^{1/4}$ and by extracting from them the data of λ/h at which $\Pi = \Pi_{\min}$ and is negative. The solid lines (1 to 5) represent these data of λ/h plotted against h/c for variety of values for $\varepsilon = 0.192$, $(W_A h^2/D)^{1/4} = 0.01$, $(0.21, 0.011)$, $(0.252, 0.0122)$, $(0.282, 0.0147)$, and $(0.35, 0.01)$, respectively. The symbols □, ◇, △, ■, and ● represent the data obtained from experiments for $\varepsilon = 0.189$ and $(W_A h^2/D)^{1/4} = 0.01$, $(0.186, 0.0114)$, $(0.166, 0.009)$, $(0.252, 0.0122)$, and $(0.133, 0.0082)$, respectively.

contact width, λ/h becomes independent of h/c as the experiment then converges to the single spacer geometry. The theory also captures our experimental observation that the amplitude does not increase from zero, but from a finite value, so that only perturbations with finite amplitude grow while others decay. However, the amplitude is somewhat overestimated, which could be due to the assumption of sinusoidal variation of the excess quantities along the y axis.

Prestretched Films

Although so far we discussed elastic films free of any prestress, here we describe our experiments with the ones subjected to uniaxial prestretching. Figure 4a–c depict the schematic in which an elastic film is first stretched along x and is then placed on a rigid substrate on which it remains strongly adhered. A flexible plate is then peeled off the film. If λ_1 is the extension ratio of the film along x, *i.e.*, $\lambda_1 = L_f/L_0$ $(\lambda_1 > 1)$, then, because of incompressibility, the extension

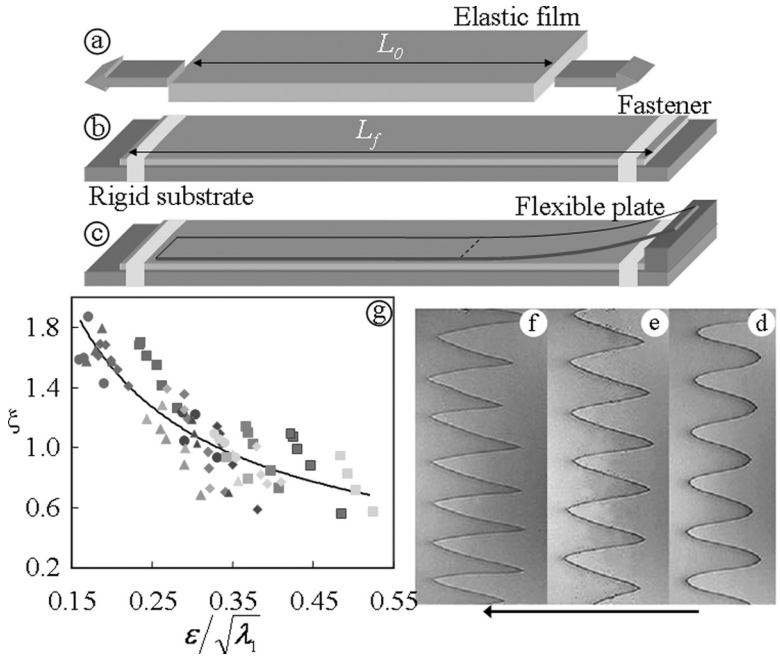

FIGURE 4 Pattern formation with prestretched films. A uniaxially stretched thin film of Sylgard® 184 (Dow Corning, Midland, MI, USA) is clamped to a rigid substrate using an adhesive tape from which a flexible plate is peeled using a spacer. (d)–(f) Videomicrographs of patterns obtained with a plate of rigidity $D = 0.02\,\text{Nm}$ and a film of modulus $\mu = 1.0\,\text{MPa}$ and thickness $h = 210\,\mu\text{m}$, stretched to $\lambda_1 = 1.4, 1.67$, and 1.87, respectively. The arrow shows the direction in which the crack opens. (g) Amplitude data from experiments with different h, D, and λ_1 are normalized as $\xi = Aq$ and are plotted against the modified confinement parameter $\varepsilon/\sqrt{\lambda_1}$. The solid curve is a guide to the eye and captures the overall variation of ξ with $\bar{\varepsilon}$.

ratio along the other two directions is $\lambda_2 = 1/\sqrt{\lambda_1}$. Video-micrographs in Figures 4d–f depict the typical examples of instability patterns that appear along the contact line. Here V-shaped fingers appear, unlike the U-shaped ones as seen in previous experiments. Although, these patterns were detected earlier by Lake *et al*. [26] during low-angle peeling of an adhesive and also by others [27] in a different context, here we study them systematically by subjecting the polymer films of different thicknesses to different extension ratios and by peeling off flexible plates of varying rigidity.

For example, in Figures 4d–f, a film with $\mu = 1.0\,\text{MPa}$ and $h = 210\,\mu\text{m}$ is progressively stretched to $\lambda_2 = 0.847, 0.774$, and 0.732,

and a plate of $D = 0.02\,\mathrm{Nm}$ is peeled from it. The resultant fingers have round tips when λ_2 is close to 1.0; however, with increasing extension of the film, the sharpness of the tip increases. Furthermore, the increase of the amplitude of the fingers with decreasing λ_2 implies that increase in pre-extension leads to longer fingers. Similar to our earlier observations, the amplitude increases also with the rigidity of the contacting plate and decreases as the thickness of the film is increased.

These features can be rationalized by considering the equilibrium of incremental stresses [28] in an incompressible elastic layer as follows (please see Appendix A for derivation):

$$\begin{aligned} &\frac{1}{\mu}\frac{\partial s}{\partial x} + \frac{1}{3}\left(\frac{2}{\lambda_1} + \lambda_1^2\right)\frac{\partial^2 u}{\partial x^2} + \frac{1}{\lambda_1}\frac{\partial^2 u}{\partial z^2} = 0, \\ &\frac{1}{\mu}\frac{\partial s}{\partial z} + \lambda_1^2\frac{\partial^2 w}{\partial x^2} + \frac{1}{3}\left(\frac{1}{\lambda_1} + 2\lambda_1^2\right)\frac{\partial^2 w}{\partial z^2} = 0. \end{aligned} \tag{21}$$

Here u and w are the incremental deformations along x and z, whereas s is the incremental average stress. Although the effect of pre-extension is intrinsically accounted for in Eq. (21), it is not amenable to analytical solutions except in the limiting situations:
$\lambda_1 \to 1$ and $\lambda_1 >> 1$. When $\lambda_1 \to 1$, long-scale approximations can be used to simplify Eq. (21) as

$$\frac{1}{\mu}\frac{\partial s}{\partial x} + \frac{1}{\lambda_1}\frac{\partial^2 u}{\partial z^2} = \frac{\partial s}{\partial z} = \frac{\partial u}{\partial x} + \frac{\partial w}{\partial z} = 0,$$

which is integrated using these conditions: perfect bonding at $z = 0$, frictionless contact, and continuity of normal stresses at $z = h/\sqrt{\lambda_1}$ (due to stretching, thickness decreases to $h/\sqrt{\lambda_1}$). This procedure yields the relation

$$\psi_0 = \frac{Dh^3}{3\mu\sqrt{\lambda_1}}\frac{\partial^6 \psi_0}{\partial x^6} \qquad \text{at } x < 0, \tag{22}$$

from which we obtain the characteristic lengths, along x: $(Dh^3/3\mu\sqrt{\lambda_1})^{1/6} \approx q^{-1}$ and along z : $h/\sqrt{\lambda_1}$. The confinement parameter $\bar{\varepsilon} = \varepsilon/\sqrt{\lambda_1}$ then implies that prestretching enhances the confinement of the film so that undulations can appear even for thicker films when they are sufficiently prestretched. The video micrographs in Figures 5a–d illustrate this situation, in which a plate of rigidity $D = 0.02\,\mathrm{Nm}$ is lifted from an elastic film ($h = 645\,\mu\mathrm{m}$ and $\mu = 1.0\,\mathrm{MPa}$). The contact line remains straight until $\lambda_1 < 1.38$, beyond which it turns undulatory. The critical value of the confinement parameter is then obtained as

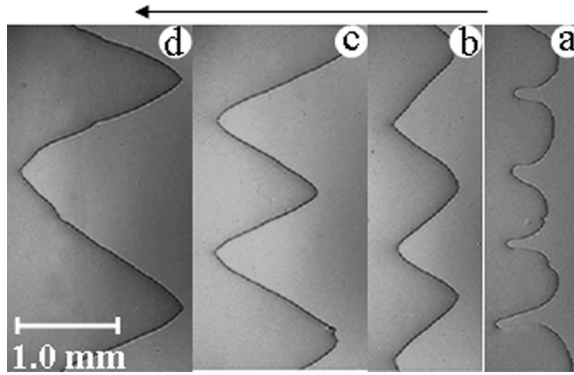

FIGURE 5 Videomicrographs of patterns observed with Sylgard® 184 elastomeric film of thickness $h = 645\,\mu\text{m}$ and shear modulus $\mu = 1.0\,\text{MPa}$, stretched to $\lambda_1 = 1.45$. Micrographs (a)–(d) are obtained with glass plates of rigidity $D = 0.02, 0.09, 0.154,$ and $0.21\,\text{Nm}$, respectively.

$\bar{\varepsilon} \approx 0.52$, which is rather large. However, in the limit of $\lambda_1 >> 1$, simplification of Eq. (21) with the assumption of constant s along z leads to

$$\psi_0 + \frac{3Dh}{\mu}\frac{\sqrt{\lambda_1}}{(\lambda_1^3 + 2)}\frac{\partial^4 \psi_0}{\partial x^4} = 0 \qquad \text{at } x < 0, \tag{23}$$

which results in a different definition, $\bar{\varepsilon} = (\mu h^3/3D)(\lambda_1^3 + 2/\sqrt{\lambda_1})^{1/4}$, and a critical value of confinement parameter $\bar{\varepsilon} = 0.36$, which is similar to our earlier observations with unstretched films ($\varepsilon = 0.35$) [14]. Furthermore the scaled amplitude $\xi = Aq$ from variety of experiments ($h = 245$–$760\,\mu\text{m}$, $\mu = 1.0\,\text{MPa}$, $D = 0.02$–$0.42\,\text{Nm}$, and $\lambda_1 = 1.45 - 1.93$) increases with decrease in $\bar{\varepsilon}$ (Figure 4g), as observed earlier. The scaled wavelength, however, does not remain constant; it increases from 2.25 to 4.25.

SUMMARY

In this report we have examined the effect of confinement of a thin elastic film *via* two different experiments in which we systematically varied the confinement by controlling the width of contact between the film and a flexible plate and by subjecting the film to pre-extension. We have characterized the confinement of the film by the ratio of two characteristic lengthscales: thickness of the film and the distance from the contact line within which the stresses remain concentrated. Whereas for experiments with semi-infinite contact width (*i.e.*, with a single spacer), the confinement parameter is obtained as

$\varepsilon = hq$, it is obtained as h/c when the contact width is finite (as in Figure 1) and $hq/\sqrt{\lambda_1}$ for prestretched films (Figure 4). We show that, in this variety of situations, the instability in the form of finger-like patterns appears at the contact line when a threshold confinement is attained, and the amplitude increases with further increase in confinement. Furthermore, in all these experiments, the amplitude increases not from zero but from a finite value. These features are all captured through our analysis in which we estimate the excess energy of the system associated with the appearance of these undulations. We show that the instability should, indeed, ensue with finite amplitude as the minima of the excess energy turns negative at a critical value of the confinement parameter. Our analysis, however, depicts a simplified picture of the very complex displacement and stress fields in the vicinity of the contact line, because, here, we consider only a single Fourier mode in describing the transverse modulations of the displacements, which fails to account for the detailed three-dimensional morphology of the interface. A full simulation of the problem coupled with a Fourier series expansion of the undulation should capture the detailed morphology of the instability patterns beyond critical confinement.

ACKNOWLEDGMENT

Part of this work constituted the PhD thesis of A. Ghatak at Lehigh University. We acknowledge the Office of Naval Research and the Pennsylvania Infrastructure Technology Alliance (PITA) for financial support.

APPENDIX

The detailed analysis of incremental deformations can be found in Reference [25] from which we obtain the stress equilibrium relations in terms of the incremental stresses in an elastic material which is already subjected to pre-stresses. Let us say that an elastic body is subjected to the initial stress field:

$$\begin{matrix} S_{11} & S_{12} & S_{13} \\ S_{12} & S_{22} & S_{23} \\ S_{13} & S_{23} & S_{33} \end{matrix}$$

where directions 1, 2 and 3 correspond to x, y and z, respectively. If the body is now deformed, a new stress field develops in the body, which when expressed with respect to the axes that rotate with the medium

can be written as,

$$\begin{matrix} S_{11}+s_{11} & S_{12}+s_{12} & S_{13}+s_{12} \\ S_{12}+s_{12} & S_{22}+s_{22} & S_{23}+s_{23} \\ S_{13}+s_{13} & S_{23}+s_{23} & S_{33}+s_{33} \end{matrix}$$

Here s_{11}, s_{22} and s_{12} etc. are the incremental stresses. In our problem, an incompressible elastic film is pre-stretched uniaxially, so that λ_1 is the extension ratio, $\lambda_1 = L_f/L_0$ ($\lambda_1 > 1$), then, due to incompressibility, the extension ratios along the other two directions are $\lambda_2 = \lambda_3 = 1/\sqrt{\lambda_1}$. Using the neo-Hookean model, the initial stress, S_{11}, in the material along direction x can be written as:

$$S_{11} = \mu\left(\lambda_1^2 - \frac{1}{\lambda_1}\right) \tag{A1}$$

The other components of the initial stresses are zero, *i.e.* $S_{12} = S_{13} = S_{23} = S_{33} = S_{22} = 0$. In the absence of body forces, the simplified form of the stress equilibrium relations (see Equation 7.49 on page 52 of Reference 25) are:

$$\begin{aligned} &\frac{\partial s_{11}}{\partial x} + \frac{\partial s_{12}}{\partial y} + \frac{\partial s_{13}}{\partial z} + S_{11}\left(\frac{\partial \omega_z}{\partial y} - \frac{\partial \omega_y}{\partial z}\right) = 0 \\ &\frac{\partial s_{12}}{\partial x} + \frac{\partial s_{22}}{\partial y} + \frac{\partial s_{23}}{\partial z} + S_{11}\frac{\partial \omega_z}{\partial x} = 0 \\ &\frac{\partial s_{13}}{\partial x} + \frac{\partial s_{23}}{\partial y} + \frac{\partial s_{33}}{\partial z} - S_{11}\frac{\partial \omega_y}{\partial x} = 0 \end{aligned} \tag{A2}$$

and the incompressibility relation is $e_{xx} + e_{yy} + e_{zz} = 0$.

The incremental stress components are expressed in terms of strains as (see Equation 8.46 on page 104 of Reference 25),

$$\begin{aligned} &s_{11} - s_{22} = \frac{2\mu}{\lambda_1}\left(e_{yy} - e_{zz}\right),\ s_{22} - s_{33} = 2\mu\left(\frac{1}{\lambda_1}e_{zz} - \lambda_1^2 e_{xx}\right) \\ &s = \frac{1}{3}\left(s_{11} + s_{22} + s_{33}\right) \\ &s_{12} = \mu\left(\lambda_1^2 + \frac{1}{\lambda_1}\right)e_{xy},\ s_{23} = \frac{2\mu}{\lambda_1}e_{yz},\ s_{31} = \mu\left(\lambda_1^2 + \frac{1}{\lambda_1}\right)e_{xz} \end{aligned} \tag{A3}$$

and, the incremental strain and rotational components are

$$
\begin{aligned}
e_{xx} &= \frac{\partial u}{\partial x},\ e_{xy} = \frac{1}{2}\left(\frac{\partial u}{\partial y} + \frac{\partial v}{\partial x}\right),\ \omega_z = \frac{1}{2}\left(\frac{\partial v}{\partial x} - \frac{\partial u}{\partial y}\right) \\
e_{yy} &= \frac{\partial v}{\partial y},\ e_{zx} = \frac{1}{2}\left(\frac{\partial w}{\partial x} + \frac{\partial u}{\partial z}\right),\ \omega_y = \frac{1}{2}\left(\frac{\partial u}{\partial z} - \frac{\partial w}{\partial x}\right) \\
e_{zz} &= \frac{\partial w}{\partial z},\ e_{yz} = \frac{1}{2}\left(\frac{\partial v}{\partial z} + \frac{\partial w}{\partial y}\right),\ \omega_x = \frac{1}{2}\left(\frac{\partial w}{\partial y} - \frac{\partial v}{\partial z}\right)
\end{aligned} \tag{A4}
$$

Using the definitions in Equations (A1), (A3) and (A4) we can rewrite Eq. (A2) as,

$$
\begin{aligned}
&\frac{\partial s}{\partial x} + \frac{\mu}{3}\left(\lambda_1^2 + \frac{2}{\lambda_1}\right)\frac{\partial^u}{\partial x^2} + \frac{\mu}{\lambda_1}\left(\frac{\partial^2 u}{\partial y^2} + \frac{\partial^2 u}{\partial z^2}\right) = 0 \\
&\frac{\partial s}{\partial y} + \mu\lambda_1^2\frac{\partial v}{\partial x^2} + \frac{\mu}{\lambda_1}\left(\frac{\partial^2 v}{\partial y^2} + \frac{\partial^2 v}{\partial z^2}\right) + \frac{2\mu}{3}\left(-\lambda_1^2 + \frac{1}{\lambda_1}\right)\frac{\partial^2 u}{\partial x \partial y} = 0 \\
&\frac{\partial s}{\partial z} + \mu\lambda_1^2\frac{\partial^2 w}{\partial x^2} + \frac{\mu}{\lambda_1}\left(\frac{\partial^2 w}{\partial y^2} + \frac{\partial^2 w}{\partial z^2}\right) + \frac{2\mu}{3}\left(-\lambda_1^2 + \frac{1}{\lambda_1}\right)\frac{\partial^2 u}{\partial x \partial z} = 0
\end{aligned} \tag{A5}
$$

In order to obtain the base solutions, we can simplify Equation A5 using the long scale approximation,

$$
\begin{aligned}
&\frac{1}{\mu}\frac{\partial s}{\partial x} + \frac{1}{3}\left(\lambda_1^2 + \frac{2}{\lambda_1}\right)\frac{\partial^u}{\partial x^2} + \frac{1}{\lambda_1}\frac{\partial^2 u}{\partial z^2} = 0 \\
&\frac{1}{\mu}\frac{\partial s}{\partial z} + \lambda_1^2\frac{\partial^2 w}{\partial x^2} + \frac{1}{3}\left(2\lambda_1^2 + \frac{1}{\lambda_1}\right)\frac{\partial^2 w}{\partial z^2} = 0
\end{aligned} \tag{A6}
$$

Equation A6 is used for analyzing the problem with pre-stretched films.

REFERENCES

[1] Saffman, P. G. and Taylor, G. I., *Proc. R. Soc. London* **A245**, 312–329 (1958).
[2] Homsy, G. M., *Annu. Rev. Fluid Mech.* **19**, 271–311 (1987).
[3] Paterson, L., *J. Fluid Mech.* **113**, 513 (1981).
[4] Nittmann, J., Daccord, G. and Stanley, H. E., *Nature* **314**, 141–144 (1985).
[5] Daccord, G., Nittmann, J. and Stanley, H. E., *Phys. Rev. Lett.* **56**, 336–339 (1986).
[6] Van Damme, H., Obrecht, F., Levitz, P., Gatineau, L. and Laroche, C., *Nature* **320**, 731–733 (1986).
[7] Reiter, G., *Phys. Rev. Lett.* **68**, 75–78 (1992).
[8] Stafford, C. M., Harrison, C., Beers, K. L., Karim, A., Amis, J. E., Vanlandingham, M. R., Kim, H.-C., Volksen, W., Miller, R. D. and Simonyi, E. E. *Nat. Mat.* **3**, 545–550 (2004).
[9] Sharp, J. S., Thomas, K. R., and Weir, M. P., *Phys. Rev. E* **75**, 011601-1–011601-11 (2007).
[10] Huang, R. and Suo, Z., *J. Appl. Phys.* **91**, 9716–9722 (2002).
[11] Ghatak, A., Chaudhury, M. K., Shenoy, V. and Sharma, A., *Phys. Rev. Lett.* **85**, 4329–4332 (2000).

[12] Mönch, W. and Herminghaus, S., *Europhys. Lett.* **53**, 525–531 (2001).
[13] Shenoy, V. and Sharma, A., *Phys. Rev. Lett.* **86**, 119–123 (2001).
[14] Ghatak, A. and Chaudhury, M. K., *Langmuir* **19**, 2621–2631 (2003).
[15] Ghatak, A., "Elastic Induced Instability in Thin Elastic Film," PhD thesis, Lehigh University, 2003.
[16] Ghatak, A., *Phys. Rev. E.* **73**, 041601-1–041601-7 (2006).
[17] Dillard, D. A., *J. Appl. Mech.* **56**, 382–386 (1989).
[18] Ghatak, A., Mahadevan, L. and Chaudhury, M. K., *Langmuir* **21**, 1277–1281 (2005).
[19] Zhang Newby, B. M. and Chaudhury, M. K., *Langmuir* **14**, 4865–4872 (1998).
[20] Maugis, D., *J. Colloid Interface Sci.* **150**, 243–269 (1992).
[21] Tang, T., Jagota, A., Chaudhury, M. K., and Hui, C.-Y., *J. Adhesion* **82**, 671–696 (2006).
[22] Hui, C.-Y., Jagota, A., Bennison, S. J. and Londono, J. D., *Proc. R. Soc. London, Ser. A* **459**, 1489–1516 (2003).
[23] Adda-Bedia, M. and Mahadevan, L. *Proc. Roy. Soc. Lond. A*, **462**(2075), 3233–3251 (2006).
[24] Oron, A., Davis, S. H. and Bankoff, S. G., *Rev. Mod. Phys.* **69**, 931–980 (1997).
[25] Sarkar, J., Shenoy, V. and Sharma, A., *Phys. Rev. Lett.* **93**, 018302-1–018302-4 (2004).
[26] Lake, G. J. and Stevenson, A., *J. Adhesion* **12**, 13–22 (1981).
[27] Evans, A. G. and Hutchinson, J. W., *Int. J. Solids Structures* **20**, 455–466 (1984); Hu, M. S., Thouless, M. D. and Evans, A. G., *Acta. Metall.* **36**, 1301–1307 (1988); Hutchinson, J. W., Thouless, M. D. and Liniger, E. G., *Acta Metall. Mater.* **40**, 295–308 (1992); Jensen, H. M. and Thouless, M. D., *Int. J. Solids Structures* **30**, 779–795 (1993); Yu, H. and Hutchinson, J. W., *Thin Solid Films* **423**, 54–63 (2003).
[28] Biot, M. A., *Mechanics of Incremental Deformations* (John Wiley & Sons, New York, 1965).